ACS APPLIED MATERIALS & INTERFACES

Research Article

www.acsami.org

Uniform Doping of Titanium in Hematite Nanorods for Efficient Photoelectrochemical Water Splitting

Degao Wang,[†] Huaican Chen,[†] Guoliang Chang,[†] Xiao Lin,[†] Yuying Zhang,[†] Ali Aldalbahi,*[,‡] Cheng Peng,*[,†] Jianqiang Wang,[†] and Chunhai Fan*[,†]

[†]Division of Physical Biology, and Bioimaging Center, Shanghai Synchrotron Radiation Facility, CAS Key Laboratory of Interfacial Physics and Technology, Shanghai Institute of Applied Physics, Chinese Academy of Sciences, Shanghai 201800, China

[‡]Chemistry Department, King Saud University, Riyadh 11451, Saudi Arabia

Supporting Information

ABSTRACT: Doping elements in hematite nanostructures is a promising approach to improve the photoelectrochemical (PEC) water-splitting performance of hematite photoanodes. However, uniform doping with precise control on doping amount and morphology is the major challenge for quantitatively investigating the PEC water-splitting enhancement. Here, we report on the design and synthesis of uniform titanium (Ti)-doped hematite nanorods with precise control of the Ti amount and morphology for highly effective PEC water splitting using an atomic layer deposition assisted solid-state diffusion method. We found that Ti doping promoted band bending and increased the carrier density as well as the surface state. Remarkably, these uniformly doped hematite nanorods exhibited high PEC performance with a pronounced photocurrent density of 2.28 mA/cm^2 at 1.23 V vs reversible hydrogen electrode (RHE) and 4.18 mA/cm^2 at 1.70 V vs RHE, respectively. Furthermore, as-prepared Ti-doping hematite nanorods performed excellent repeatability and durability; over 80% of the as-fabricated photoanodes reproduced the steady photocurrent density of 1.9−2.2 mA/cm^2 at 1.23 V vs RHE at least 3 h in a strong alkaline electrolyte solution.

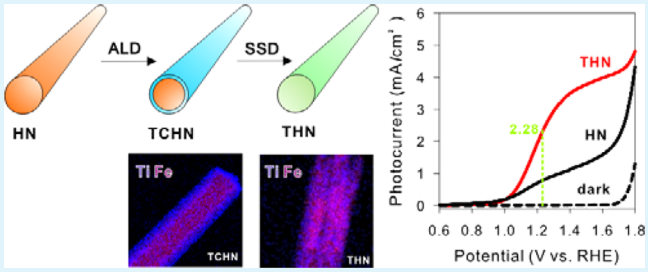

KEYWORDS: *uniform Ti doping, hematite nanorod, photoelectrochemical, atomic layer deposition, solid-state diffusion*

INTRODUCTION

Photoelectrochemical (PEC) water splitting holds great promise for sustainable energy by harvesting solar energy in a cost-effective fashion using earth-abundant materials.[1,2] Hematite (α-Fe_2O_3) is an attractive candidate for PEC photoanode material because it has a favorable bandgap of about 2.2 eV, allowing a maximum theoretical solar-to-hydrogen efficiency of 16.8% under air mass (AM) 1.5 G illumination.[3,4] Nevertheless, the efficiency of hematite-based PEC is far from the theoretical values, owing to its very short excited-state life, short hole diffusion length, poor surface oxygen evolution reaction kinetics, and poor electrical conductivity.[5] Currently, introducing impurities into hematite nanostructures has been extensively studied to improve PEC performance via optimizing the structural, electronic, and optical properties.[6−9] Particularly, Ti doping largely enhanced the PEC performance of hematite nanorods, which was attributed to improved donor density and reduced the electron−hole recombination rate.[10−13] Despite the rapid advances in this direction, it remains a great challenge to approach the theoretical efficiency limit of hematite-based PEC. It is envisioned that better control of the Ti-doping amount and morphology should be beneficial to the PEC performance.[14]

Vertically aligned hematite nanorods (HNs) are highly attractive materials for PEC water splitting since they can be facilely fabricated using chemical bath deposition (CBD) and possess unique morphology for hole diffusion.[15−20] There has been considerable interest in efficient doping of HNs. Direct introduction of Ti ions in the CBD process and solid-state diffusion (SSD) are two main approaches for Ti doping in HNs. In the former approach, Ti atoms are embedded in the crystal lattice of HNs with inefficient control of the doping amounts.[13] Whereas increasing the amount of Ti doping should improve the PEC performance, the morphology of HNs is often unfavorably altered, which lowers the water-splitting efficiency.[10,11,14] SSD provides an alternative approach to Ti doping on HNs in large amounts. However, Ti-contained precursors are often deposited on the HN surface, which subsequently diffuse into HNs after high-temperature post-treatment. This process often results in the formation of irregular films with uncontrollable thickness on HNs.[21−23] In addition to the efficiency loss, morphology change and

Received: April 16, 2015
Accepted: June 8, 2015
Published: June 8, 2015

DOI: 10.1021/acsami.5b03298
ACS Appl. Mater. Interfaces 2015, 7, 14072−14078

nonuniform Ti doping are also prominent factors for the reproducibility and reusability of PEC.

In this work, we developed an atomic layer deposition (ALD)-assisted approach to uniform-dope HNs with Ti atoms in a controllable and quantitative manner. ALD is a powerful technique for producing uniform coatings on arbitrary-shaped substrates with atomic-scale control.[24−27] For example, ultrathin hematite-coated tin oxide nanocones exhibit nearly total solar absorption,[28] and ultrathin cobalt oxide-deposited layer significantly enhanced photoelectrochemical water oxidation performance.[29] Very recently, Yang and co-workers fabricated uniform Mn-doped TiO_2 nanorods by using ALD in the SSD process.[30] However, whereas Mn was completely incorporated into TiO_2 nanorods with little morphology change, the photocurrent density of TiO_2 nanorods was decreased after Mn doping, possibly because the mid gap state formed by transition-metal dopant are acting as recombination centers. Interestingly, we find that our ALD-assisted method led to HNs with uniform Ti doping and minimal morphology variation. Thus, prepared HNs exhibited superior PEC water-splitting efficiency and high robustness for repeated use.

EXPERIMENTAL DETAILS

Preparation of Hematite Nanorods. Hematite nanorods are prepared by following a traditional hydrothermal method in the literature.[20] In a typical preparation, 0.15 M $FeCl_3$ and 0.15 M urea were first dissolved in aqueous solution as the precursor solution. A Teflon-lined stainless autoclave was filled with 20 mL of precursor solution, and a piece of fluorine-doped tin oxide (FTO) glass slide was then put into the autoclave "upside down". After a thermal treatment at 100 °C in a box oven for 12 h, a uniform yellow color β-FeOOH film was coated on the FTO glass. The obtained β-FeOOH-coated FTO glass was then rinsed with deionized water three times for complete removal of the residual salts. Subsequently, the yellow β-FeOOH film on FTO glass was transformed into orange red hematite nanorods after an annealing treatment at 500 °C in a preheated furnace for 1 h.

Ti Doping on Hematite Nanorods. The area of FTO substrate without hematite nanorods were coated with 3M tape for later forming ohm contact during the fabrication of electrode. $TiCl_4$ and water were utilized as the precursors and held in a customized bubbler at room temperature. The typical pulse time for the titanium precursors and water were 0.05 and 0.025 s, respectively. Ti_xO_y film deposition was performed in a thermal ALD reactor (Kemin T-200L) at 150 °C. The obtained Ti_xO_y-coated hematite nanorods were then loaded into a preheated furnace at 700 °C for 30 min to complete solid-state diffusion. As the control experiments, the hematite nanorods without Ti doping were also treated at 700 °C for 30 min in a preheated furnace.

Co^{2+} Modification. The as-prepared Ti-doped hematite nanorods were soaked in 10 mM $Co(NO_3)_2$ aqueous solution for 10 s and then rinsed with deionized water two times. After drying with nitrogen gas (99.99%), the procedure above was repeated one time for completely covering Co^{2+} on Ti-doped hematite nanorods.

Material Characterization. The morphologies of all samples were characterized with a scanning electron microscope (SEM, JME2011, JEOL, Japan) and a high-resolution transmission electron microscope (HRTEM, FEI TECNAI G^2 F20). TEM samples were prepared by scrapping the hematite nanorods from the FTO with a new blade. Then the powders were carefully transferred to the EP tube and dispersed by methanol (high-performance liquid chromatography class). X-ray diffraction spectra (XRD) were carried out with an X-ray diffractometer (Bruker AXS, D8 Advanced) using Cu Kα radiation (λ = 1.5418 Å). X-ray photoelectron spectra (XPS) were carried out with a PerkinElmer 1257 model, operating at an average base pressure of ~5.9×10^{-9} Torr at 300 K with a non-monochromatized Al Kα line at 1486.6 eV and a hemispherical sector analyzer with resolution of 25 meV. Electrochemical impedance spectra (EIS) were collected with an Autolab electrochemical workstation (Metrohm AG, Switzerland).

Electrochemical Characterization. Hematite photoanode was first fabricated by sealing a part of the hematite-covered FTO electrode (including the edges) with epoxy resin except for the 0.25 cm^2 unsealed area left for photoexcitation; an external Cu wire was connected to the FTO surface using a 63/37 Sn/Pb solder from Youbang Soldering Company, Hangzhou, China. An Autolab electrochemical station with Nova electrochemical software was then employed to study the electrochemical properties and stability of the as-fabricated photoanodes in a three-electrode electrochemical cell. Impedance spectra were collected using a 10 mV amplitude perturbation between 100 kHz and 0.01 Hz and Z-view software was adopted to fit these data. All of the photoanodes were tested under illumination on the FTO side.

PEC Measurements. The PEC activity was measured using line scan voltammetry in a standard three-electrode setup. The hematite on FTO was regarded as the working electrode, a platinum plate as the counter electrode, and Ag/AgCl as the reference electrode. All measurements were conducted in a 1 M NaOH electrolyte (pH 13.6). The photocurrent density of each photoanode was recorded by the Autolab electrochemical station under 100 mW/cm^2 provide by a 500 W Xe lamp (Newport, Model SP 94023A) with an AM 1.5 G filter (AM 1.5G). Before the measurement, light intensity was standardized using a calibrated silicon photodiode (Newport, 91150 V). Incident photon-to-current efficiency (IPCE) spectra were measured at 1.23 V vs RHE as a function of the wavelength of the incident light by an electrochemical station (CHI 650b) with a solar simulator (Newport 66902, 500 W xenon lamp), coupled to an aligned monochromator (Newport 74125) and a Si detector (Newport 71675). The IPCE values are calculated by IPCE = $(1240I)/(\lambda J_{light})$, where I is the photocurrent density (mA/cm^2), λ is the incident light wavelength (nm), and J_{light} is the power density of monochromatic light at a specific wavelength.

RESULTS

Synthesis and Characterization. Uniform Ti-doped hematite nanorods were developed as photoanodes by a simple and inexpensive method for efficient PEC water splitting. Figure 1a shows the procedure for uniform Ti doping on hematite nanorods. First, vertically aligned hematite nanorod arrays (dubbed HN) were prepared by chemical bath

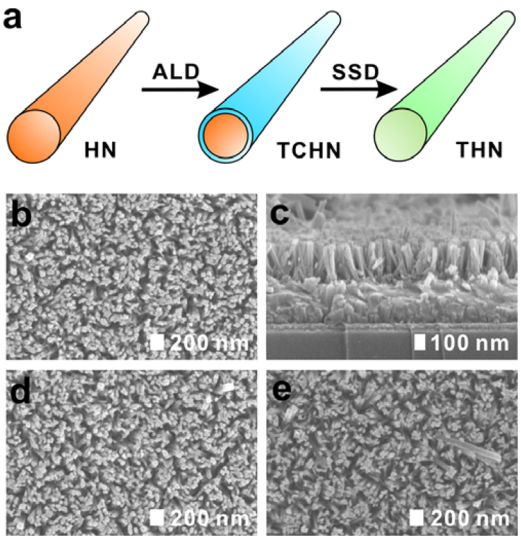

Figure 1. Scanning electron microscopy images: (a) Schematic illustration of the preparation of uniform Ti-doped hematite nanorods. (b, c) Top-view and cross-sectional-view images of THN, respectively. (d, e) Top-view images of TCHN and HN, respectively.

DOI: 10.1021/acsami.5b03298
ACS Appl. Mater. Interfaces 2015, 7, 14072−14078

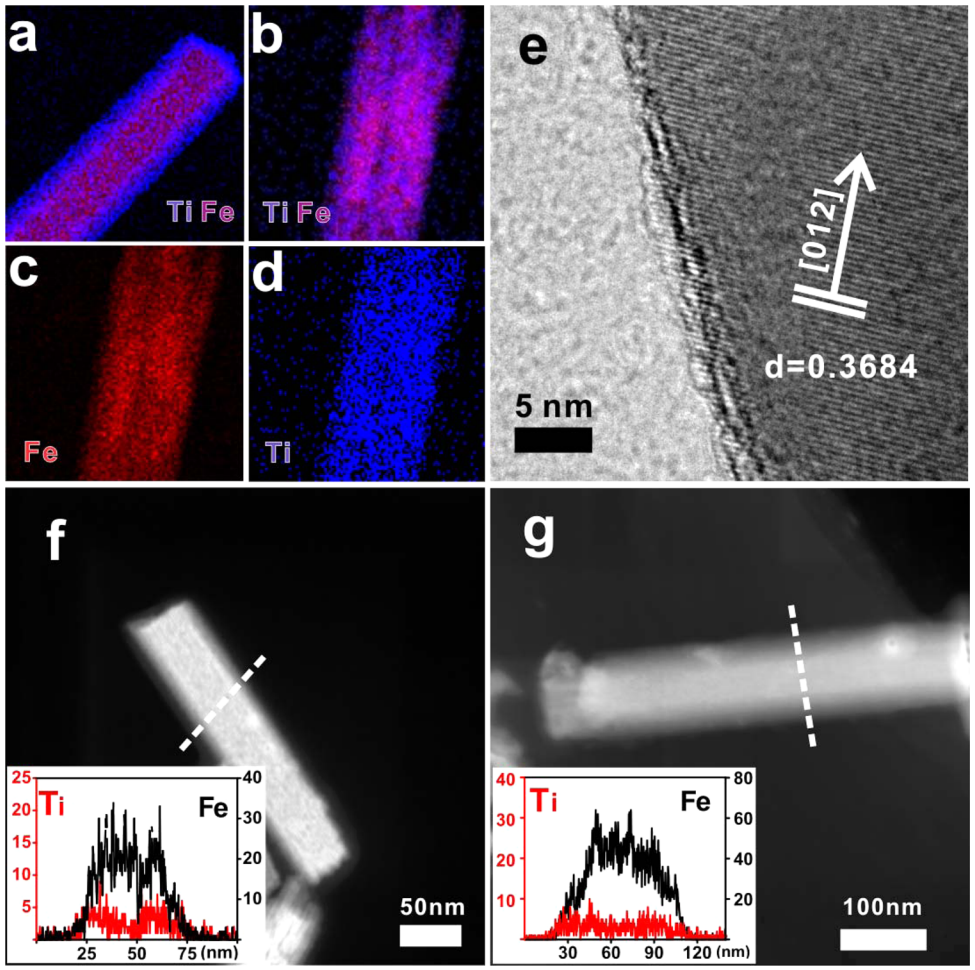

Figure 2. Ti-distribution characterization: (a) Ti distribution and Fe distribution in TCHN. (b) Ti distribution and Fe distribution in THN. (c) Fe distribution in THN. (d) Ti distribution in THN. (e) HRTEM image of THN. (f) TEM image of TCHN; the inset plots are Fe and Ti line scans across the diameter of the nanorod. (g) TEM image of THN; the inset plots are Fe and Ti line scans across the diameter of the nanorod.

deposition (CBD) with an annealing treatment at 500 °C.[19] Second, water and $TiCl_4$ were utilized as the precursors in the ALD process for depositing ultrathin Ti_xO_y layer on hematite nanorods with a tunable thickness on the angstrom scale. Then the as-obtained conformal Ti_xO_y-coated hematite nanorods (dubbed TCHN) were loaded into a preheated furnace at 700 °C to complete the SSD process for producing uniform Ti-doped hematite nanorods (dubbed THN). The concentrations of Ti doping were precisely controlled by the number of cycles in the ALD process.

We first studied the morphology and structure of uniform Ti-doped hematite nanorod arrays on FTO substrate. Figure 1c shows the average length and diameter of THN are ~400 and ~50 nm, respectively. All of the THNs (Figure 1b) are vertically aligned on the FTO substrate, similar to TCHN (Figure 1d) and HN (Figure 1e). It indicates that the one-dimensional (1D) rodlike morphology is well-retained after the ALD and SSD process. Importantly, this is the first report on Ti-doped hematite nanorods with excellent 1D structure on FTO substrate after 700 °C annealing treatment. The XRD pattern of THN (Figure S1) further reveals that THN photoanode contains two phases of hematite and cassiterite, but is absente of anatase or rutile titanium dioxide. It indicates that the Ti_xO_y shell has completely incorporated into hematite nanorods.

Further, we collected XPS to elucidate the electronic structure of THN. Apparently, the Ti $2p_{3/2}$ binding energy is 458.2 eV (Figure S2a), differing from the typical Ti metal (454.2 eV) and TiO_2 (459.0 eV). It indicates that the Ti atoms have incorporated into the crystal structure of hematite. Furthermore, the present Fe $2p_{3/2}$ peak at 710.3 eV and the absent satellite peak at 715.5 eV in Fe 2p XPS spectra (Figure S2b) implies that Ti incorporation has little influence on Fe^{3+} in hematite nanorods. Of note, O 1s XPS spectra in Figure S2c shows that the binding energy of the main line shifts from 529.5 eV in HN to 529.9 eV in THN, confirming that Ti atoms have successfully doped into the lattice of hematite.[21]

Next, we investigated Ti distribution in TCHN and THN using transmission electron microscopy (TEM), high-resolution TEM (HRTEM), and scanning transmission electron microscopy mode-energy dispersive spectroscopy (EDS) mapping measurements. Figure 2a shows that TCHN is Ti_xO_y-coated hematite nanorods with a conformal core/shell structure; most of the Ti atoms are deposited on the surface of hematite nanorods. The line scan across the diameter of TCHN (Figure 2f, inset) further illustrates that the Ti-distribution curve is low in the middle, indicating that Ti atoms are distributed on the surface of hematite nanorods. In contrast, the Ti-distribution curve in THN is a straight line (Figure 2g, inset), indicating Ti atoms have incorporated into hematite

DOI: 10.1021/acsami.5b03298
ACS Appl. Mater. Interfaces 2015, 7, 14072−14078

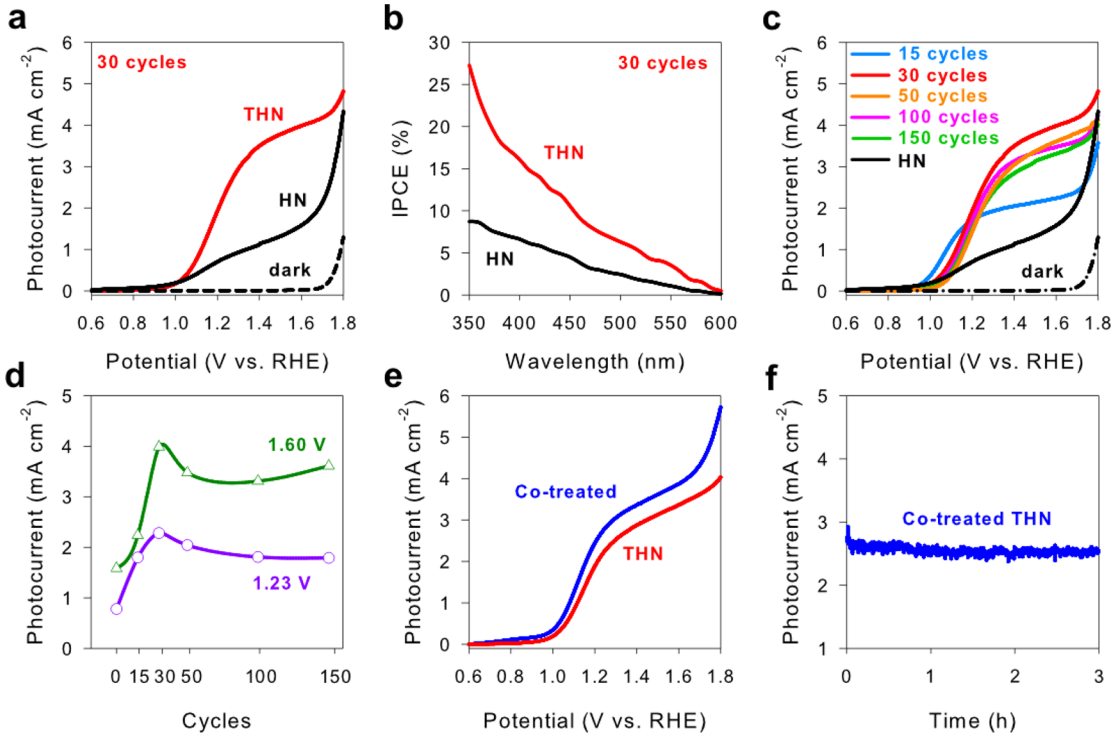

Figure 3. PEC performances: (a) *J*–*V* curves of THN and HN with 30 ALD cycles. (b) IPCE spectra at 1.23 V vs RHE of HN and THN with 30 ALD cycles in a 1 M NaOH electrolyte (pH 13.6), respectively. (c) *J*–*V* curves of THN with different ALD cycles. (d) Photocurrent values of THN with different ALD cycles at 1.23 and 1.60 V vs RHE, respectively. (e) *J*–*V* curves of THN after Co treatment. (f) *J*–*t* curve of THN with Co treatment.

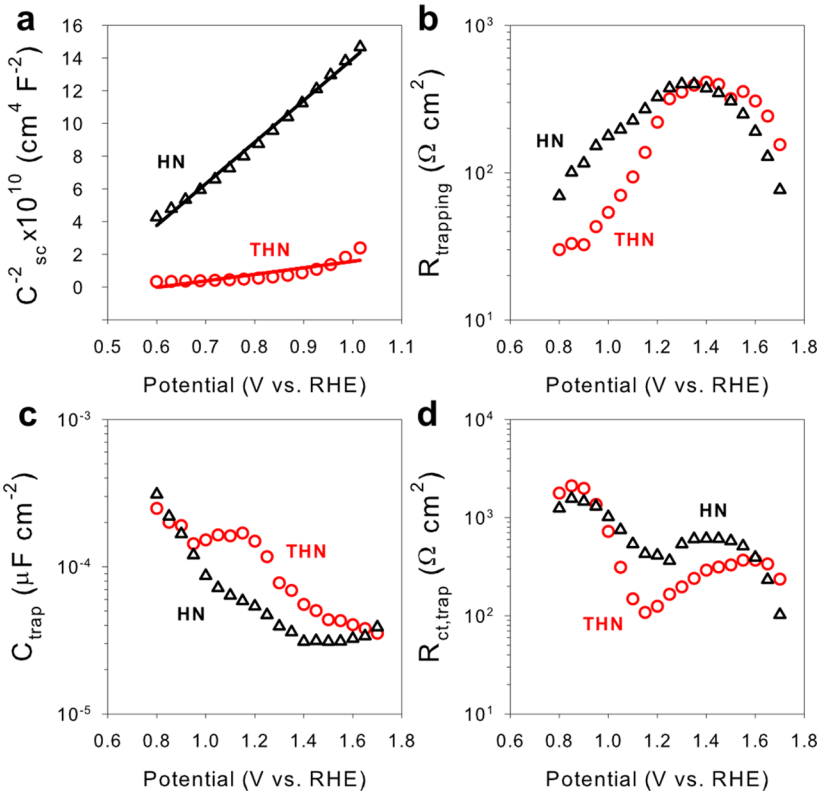

Figure 4. Charge separation and transfer: (a) Mott–Schottky plots of THN and HN, respectively. (b) Plot of $R_{trapping}$, (c) C_{trap}, and (d) $R_{ct,trap}$ obtained from fitting EIS data upon illumination.

nanorods after high-temperature treatment in the SSD process. EDS mapping of THN (Figure 2b) further demonstrates Ti atoms have uniformly distributed in hematite nanorods, instead of depositing on the surface of TCHN. The HRTEM image of

DOI: 10.1021/acsami.5b03298
ACS Appl. Mater. Interfaces 2015, 7, 14072–14078

THN (Figure 2e) reveals the interplanar spacing of (012) is 0.3684 nm, which is very consistent with that of JCPDS 33-0664. It strongly indicates that Ti incorporation has little influence on the structure of hematite nanorods.

PEC Performance. To evaluate the effect of Ti doping on PEC performance, we performed PEC measurements in 1 M NaOH electrolyte using a three-electrode electrochemical cell under simulated sunlight irradiation (100 mW/cm^2, AM 1.5 G). As shown in Figure 3a, the photocurrent density of THN with 30 ALD cycles reached 2.28 mA/cm^2 at 1.23 V vs RHE, ~3 times higher than that of HN. Furthermore, this pronounced effect of Ti-doped hematite nanorods was found to be highly reproducible; over 80% of the photocurrent densities of 1.9−2.2 mA/cm^2 at 1.23 V vs RHE were reproduced in 30 as-fabricated photoanodes. More impressive, the photocurrent value of THN even reached 4.18 mA/cm^2 at 1.70 V vs RHE before photocurrent increased exponentially. To the best of our knowledge, this is the highest photocurrent density ever achieved by Ti-doped hematite nanorods. Correspondingly, we further examined the IPCE as a function of incident light wavelength (Figure 3b).[31−33] THN with 30 ALD cycles shows substantially enhanced IPCE values compared to HN over the entire wavelength from 350 to 600 nm, which are consistent with their photocurrent−potential (J−V) characteristics. THN yielded the maximum IPCE value of 27.3% at the wavelength of 350 nm, ~3 times higher than of 8.72% of HN measured at 1.23 V vs RHE. IPCE values of both THN and HN gradually dropped to zero at wavelengths above 600 nm, in accordance with the bandgap of hematite.

We turn now to consideration of the effects of Ti-doping amounts on the PEC performance of THN. Figure 3c shows J−V curves of the HN and THN with different Ti-doping concentrations. The dark current densities in all cases can be negated. It was found that Ti-doping concentration gave rise to a strong effect on the J−V characteristics. The photocurrent densities increased from 0.78 of HN (without Ti doping) to 1.80, 2.28, 2.04, 1.81, and 1.79 mA/cm^2 at 1.23 V vs RHE with 15, 30, 50, 100, and 150 cycles of ALD treatments, respectively. Figure 3d reveals that THN reached the maximum photocurrent density at 1.23 V vs RHE when Ti_yO_x deposition was 30 ALD cycles, further increasing ALD deposition to 50 cycles, resulting in a slight decrease of the photocurrent. It indicates that the effects of Ti doping reached saturation at the point of 30 ALD cycles. The same trend was observed when the bias voltage was 1.60 V vs RHE. Moreover, the onset potentials of all THNs are identical to that of HN (~0.9 V vs RHE), indicating that Ti doping has little influence on the surface of hematite nanorods.

Charge Separation and Transfer. To understand the mechanism of Ti-doping enhancement, we exploited the electrochemical impedance spectroscopy (EIS) of both THN and HN. Capacitances were obtained from the EIS spectra at each potential with a frequency of 10 Hz in the dark, for generating Mott−Schottky plots (Figure 4a). We thus estimated the carrier density in THN is 1.49 × 10^{19} cm^{-3}, 2 orders of magnitude higher than that of HN (4.05 × 10^{17} cm^{-3}). It indicates that Ti doping largely increased the carrier density in hematite nanorods. Mott−Schottky plots further demonstrate that the flat band potential (V_{fp}) of THN is 0.4 V vs RHE, larger than 0.3 V vs RHE of HN. Such anodic shift of V_{fp} indicates that Ti doping promotes band bending, thus accelerating the charge separation and increasing the number of carriers.[34]

We further collected the EIS spectra to investigate the charge separation and transfer at the electrode/electrolyte interface. Given that the surface state serves as the hole-trapping center for charge separation and transfer upon illumination,[24,35,36] the Nyquist diagrams of both THN and HN were molded by a surface-state-based equivalent circuit (Figure S4) to calculate the EIS data. Compared with HN, Ti doping leads to the decrease of $R_{trapping}$ (the resistance for trapping holes in the surface states) and the increase of C_{trap} (the capacitance to trap holes in the surface state), as shown in parts b and c of Figure 4, respectively . The former facilitates trapping holes in surface states, and the latter indicates more holes were trapped for participating water oxidation, with both of them facilitating charge separation. Moreover, Figure 4d shows that the $R_{ct,trap}$ (the charge-transfer resistance from surface states to electrolyte) of THN is smaller than that of HN, indicating that Ti doping facilitates charge transfer across the electrode/electrolyte.

Co^{2+} Treatment. Considering that the onset potential (0.9 V vs RHE) of THN is so much larger than the flat band potential (0.4 V vs RHE), we employed cobalt treatment to further improve the PEC water splitting performance.[37] Figure 3e shows that the onset potential of THN (with 30 ALD cycles) has a remarkable 0.08 V cathodic onset potential shift after Co^{2+} treatment. Simultaneously, the photocurrent response was improved by Co^{2+} treatment from 2.13 to 2.68 mA/cm^2 at 1.23 V vs RHE, which is comparable to the benchmark responses of Co^{2+} treated Si-doped dendritic hematite photoanodes. Moreover, we have performed amperometric J−t studies at the bias voltage of 1.23 V vs RHE under illumination to evaluate the photoresponse of cobalt-treated THN over time. Figure 3f shows that the photocurrent density of Co-treated THN remains at ~2.6 mA/cm^2 for at least 3 h, and Figure S3 shows the photocurrent density of THN remains at ~2.1 mA/cm^2. Both of them indicate that it is stable in a NaOH aqueous solution (pH 13.6), though with an initial slight decrease before stabilization.

DISCUSSION

Titanium incorporation is known to enhance the efficiency in hematite nanostructures. Especially, uniform Ti doping is critical for reproducibility and reusability for PEC performance enhancement and quantitative mechanism investigation. However, previous efforts on Ti doping were highly synthesis-dependent, which led to complicated mechanisms for PEC enhancement due to the lack of precise control of the Ti-doping amount and morphology.[14] In the current work, we successfully synthesized uniform Ti-doped hematite nanorod arrays with efficient PEC water-splitting performance, using ALD-assisted SSD. The as-fabricated Ti-doped hematite nanorod holds a promising morphological structure with a diameter of 50 nm and length of 400 nm, which is very close to the ideal morphology of vertically aligned hematite nanorod arrays (with a feature diameter of ca. 20 nm and length of ca. 400 nm) that offers a continuous path for electron transport and high efficiency for photon harvesting.[23] In such ALD-assisted SSD process, Ti_xO_y conformal ultrathin films were deposited on hematite nanorods for confining the morphology of hematite nanorods and providing Ti sources during high-temperature annealing treatment. We found that all Ti atoms were rapidly diffused and uniformly distributed in hematite nanorods after high-temperature diffusion equilibrium; thus, no residues were left on the surface of hematite nanorods. It firmly

DOI: 10.1021/acsami.5b03298
ACS Appl. Mater. Interfaces 2015, 7, 14072−14078

indicates that Ti-doping amounts in ALD-assisted SSD were precisely controlled by the number of ALD cycles. In contrast, Ti-doping amounts lack precise control in the traditional SSD process or introducing Ti ions in the CBD process. Furthermore, Ti_xO_y conformal ultrathin films are sufficient to confine the morphology of hematite nanorods because Ti diffusion is directed from the exterior to the interior driven by high-temperature post-treatment.

The major advantage of the ALD-assisted SSD process for Ti doping on hematite nanorods is the absence of morphology change and surface residues, which significantly simplifies the mechanism of PEC performance enhancement. The lack of surface residues precludes the possibility that the increased carrier density is attributed to the enhanced charge separation by heterostructures formed on the surface hematite nanorods.[38] Also, since the morphology does not change, the increased carrier density should not come from morphological evolution.[23] Moreover, XPS spectra revealed the absence of Fe^{2+} in THN, precluding the hopping mechanism for the increase of carrier density.[15] Therefore, quantitative investigation in Figure 4a demonstrates that the photocurrent densities of THN are increased with the Ti amounts, strongly suggesting that the largely improved PEC performance of hematite nanorods should be attributed to Ti doping. Figure 4a further demonstrates the photocurrent density reached a maximum value of 4.18 mA/cm^2 at 1.70 V vs RHE when the Ti amount was 30 ALD cycles, whereas further increasing the Ti amount slightly decreased photocurrent density. It indicates that excess Ti doping does not further improve the PEC performance, which is very consistent with the results reported by Jin and co-workers.[22]

CONCLUSION

We have successfully synthesized uniform Ti-doped hematite nanorods for efficient PEC water splitting via an ALD-assisted SSD method. Because of precise control of the Ti amount, there are no surface residues or morphology change occurring on the hematite nanorods. As a result, we obtained a photocurrent density of 4.18 mA/cm^2 at 1.70 V vs RHE under a standard AM 1.5 G solar light simulator, representing the highest photocurrent density ever achieved by Ti-doped hematite nanorods. Co^{2+} treatment further improved the photocurrent density from 2.13 to 2.68 mA/cm^2 at 1.23 V vs RHE, which is comparable to the benchmark of Si-doped hematite nanostructures designed by Grätzel eand co-workers.[39] Because of the absence of surface residues and morphology change, quantitative investigation of Ti amounts revealed that Ti doping promoted band bending and largely increased the carrier density as well as the surface state, thus significantly enhancing the PEC water-splitting performance of hematite nanorods. Moreover, such uniform Ti-doped hematite nanorods have excellent repeatability and durability; over 80% of the as-fabricated photoanodes reproduced the steady photocurrent density of 1.9−2.2 mA/cm^2 at 1.23 V vs RHE at least 3 h in strong alkaline electrolyte solution. Therefore, we believe that there is still much room for achieving more significant PEC performance after further treatments such as codoping and heterojunction.

ASSOCIATED CONTENT

Supporting Information

XRD and XPS data, $J-t$ curve of THN, and equivalent circuit for fitting EIS data. The Supporting Information is available free of charge on the ACS Publications website at DOI: 10.1021/acsami.5b03298.

AUTHOR INFORMATION

Corresponding Authors

*E-mail: aaldalbahi@ksu.edu.sa (A.A.).
*E-mail: pengcheng@sinap.ac.cn (C.P.).
*E-mail: fchh@sinap.ac.cn (C.F.).

Notes

The authors declare no competing financial interest.

ACKNOWLEDGMENTS

We acknowledge financial support from the National Natural Science Foundation 51102272 and 91127001, Research Fund from King Saud University, and Foundation of State Key Laboratory of Coal Combustion FSKLCC1209.

REFERENCES

(1) Fujishima, A.; Honda, K. Electrochemical Photolysis of Water at a Semiconductor Electrode. *Nature* **1972**, *238*, 37−38.
(2) Gratzel, M. Photoelectrochemical Cells. *Nature* **2001**, *414*, 338−344.
(3) Sivula, K.; Le Formal, F.; Gratzel, M. Solar Water Splitting: Progress Using Hematite (α-Fe_2O_3) Photoelectrodes. *ChemSusChem* **2010**, *4*, 432−449.
(4) Li, Y.; Zhang, J. Z. Hydrogen Generation from Photoelectrochemical Water Splitting Based on Nanomaterials. *Laser Photonics Rev.* **2010**, *4*, 517−528.
(5) Ling, Y.; Li, Y. Review of Sn-Doped Hematite Nanostructures for Photoelectrochemical Water Splitting. *Part. Part. Syst. Charact.* **2014**, *31*, 1113−1121.
(6) Wheeler, D. A.; Wang, G. M.; Ling, Y. C.; Li, Y.; Zhang, J. Z. Nanostructured Hematite: Synthesis, Characterization, Charge Carrier Dynamics, and Photoelectrochemical Properties. *Energy Environ. Sci.* **2012**, *5*, 6682−6702.
(7) Qin, D.-D.; Tao, C.-L.; In, S.-i.; Yang, Z.-Y.; Mallouk, T. E.; Bao, N.; Grimes, C. A. Facile Solvothermal Method for Fabricating Arrays of Vertically Oriented α-Fe_2O_3 Nanowires and Their Application in Photoelectrochemical Water Oxidation. *Energy Fuels* **2011**, *25*, 5257−5263.
(8) Mirbagheri, N.; Wang, D.; Peng, C.; Wang, J.; Huang, Q.; Fan, C.; Ferapontova, E. E. Visible Light Driven Photoelectrochemical Water Oxidation by Zn and Ti-doped Hematite Nanostructures. *ACS Catal.* **2014**, *4*, 2006−2015.
(9) Sun, Y. Q.; Chemelewski, W. D.; Berglund, S. P.; Li, C.; He, H. C.; Shi, G. Q.; Mullins, C. B. Antimony-Doped Tin Oxide Nanorods as a Transparent Conducting Electrode for Enhancing Photoelectrochemical Oxidation of Water by Hematite. *ACS Appl. Mater. Interfaces* **2014**, *6*, 5494−5499.
(10) Deng, J. J.; Zhong, J.; Pu, A. W.; Zhang, D.; Li, M.; Sun, X. H.; Lee, S. T. Ti-Doped Hematite Nanostructures for Solar Water Splitting with High Efficiency. *J. Appl. Phys.* **2012**, *112*, 084312.
(11) Shen, S. H.; Kronawitter, C. X.; Wheeler, D. A.; Guo, P. H.; Lindley, S. A.; Jiang, J. G.; Zhang, J. Z.; Guo, L. J.; Mao, S. S. Physical and Photoelectrochemical Characterization of Ti-Doped Hematite Photoanodes Prepared by Solution Growth. *J. Mater. Chem. A* **2013**, *1*, 14498−14506.
(12) Fu, Z. W.; Jiang, T. F.; Zhang, L. J.; Liu, B. K.; Wang, D. J.; Wang, L. L.; Xie, T. F. Surface Treatment with Al^{3+} on a Ti-Doped α-Fe_2O_3 Nanorod Array Photoanode for Efficient Photoelectrochemical Water Splitting. *J. Mater. Chem. A* **2014**, *2*, 13705−13712.
(13) Fu, Z. W.; Jiang, T. F.; Liu, Z. P.; Wang, D. J.; Wang, L. L.; Xie, T. F. Highly Photoactive Ti-Doped α-Fe_2O_3 Nanorod Arrays Photoanode Prepared by a Hydrothermal Method for Photoelectrochemical Water Splitting. *Electrochim. Acta* **2014**, *129*, 358−363.
(14) Kronawitter, C. X.; Zegkinoglou, I.; Shen, S. H.; Liao, P.; Cho, I. S.; Zandi, O.; Liu, Y. S.; Lashgari, K.; Westin, G.; Guo, J. H.; Himpsel,

DOI: 10.1021/acsami.5b03298
ACS Appl. Mater. Interfaces 2015, 7, 14072−14078

F. J.; Carter, E. A.; Zheng, X. L.; Hamann, T. W.; Koel, B. E.; Mao, S. S.; Vayssieres, L. Titanium Incorporation into Hematite Photoelectrodes: Theoretical Considerations and Experimental Observations. *Energy Environ. Sci.* **2014**, *7*, 3100−3121.
(15) Morrish, R.; Rahman, M.; MacElroy, J. M. D.; Wolden, C. A. Activation of Hematite Nanorod Arrays for Photoelectrochemical Water Splitting. *ChemSusChem* **2011**, *4*, 474−479.
(16) Vayssieres, L.; Beermann, N.; Lindquist, S. E.; Hagfeldt, A. Controlled Aqueous Chemical Growth of Oriented Three-dimensional Crystalline Nanorod Arrays: Application to Iron(III) Oxides. *Chem. Mater.* **2001**, *13*, 233−235.
(17) Wang, P.; Wang, D. G.; Lin, J.; Li, X. L.; Peng, C.; Gao, X. Y.; Huang, Q.; Wang, J. Q.; Xu, H. J.; Fan, C. H. Lattice Defect-Enhanced Hydrogen Production in Nanostructured Hematite-based Photoelectrochemical Device. *ACS Appl. Mater. Interfaces* **2012**, *4*, 2295−2302.
(18) Li, J. T.; Cushing, S. K.; Zheng, P.; Meng, F. K.; Chu, D.; Wu, N. Q. Plasmon-Induced Photonic and Energy-Transfer Enhancement of Solar Water Splitting by a Hematite Nanorod Array. *Nat. Commun.* **2013**, *4*, 2651.
(19) de Carvalho, W. M.; Souza, F. L. Recent Ddvances on Solar Water Splitting Using Hematite Nanorod Film Produced by Purpose-Built Material Methods. *J. Mater. Res.* **2014**, *29*, 16−28.
(20) Xi, L. F.; Chiam, S. Y.; Mak, W. F.; Tran, P. D.; Barber, J.; Loo, S. C. J.; Wong, L. H. A Novel Strategy for Surface Treatment on Hematite Photoanode for Efficient Water Oxidation. *Chem. Sci.* **2013**, *4*, 164−169.
(21) Wang, G. M.; Ling, Y. C.; Wheeler, D. A.; George, K. E. N.; Horsley, K.; Heske, C.; Zhang, J. Z.; Li, Y. Facile Synthesis of Highly Photoactive α-Fe_2O_3-Based Films for Water Oxidation. *Nano Lett.* **2011**, *11*, 3503−3509.
(22) Franking, R.; Li, L. S.; Lukowski, M. A.; Meng, F.; Tan, Y. Z.; Hamers, R. J.; Jin, S. Facile Post-growth Doping of Nanostructured Hematite Photoanodes for Enhanced Photoelectrochemical Water Oxidation. *Energy Environ. Sci.* **2013**, *6*, 500−512.
(23) Brillet, J.; Gratzel, M.; Sivula, K. Decoupling Feature Size and Functionality in Solution-Processed, Porous Hematite Electrodes for Solar Water Splitting. *Nano Lett.* **2010**, *10*, 4155−4160.
(24) Prasittichai, C.; Avila, J. R.; Farha, O. K.; Hupp, J. T. Systematic Modulation of Quantum (Electron) Tunneling Behavior by Atomic Layer Deposition on Nanoparticulate SnO_2 and TiO_2 Photoanodes. *J. Am. Chem. Soc.* **2013**, *135*, 16328−16331.
(25) Zandi, O.; Beardslee, J. A.; Hamann, T. Substrate Dependent Water Splitting with Ultrathin α-Fe_2O_3 Electrodes. *J. Phys. Chem. C* **2014**, *118*, 16494−16503.
(26) Yang, X. G.; Liu, R.; Du, C.; Dai, P. C.; Zheng, Z.; Wang, D. W. Improving Hematite-Based Photoelectrochemical Water Splitting with Ultrathin TiO_2 by Atomic Layer Deposition. *ACS Appl. Mater. Interfaces* **2014**, *6*, 12005−12011.
(27) Wang, T.; Luo, Z. B.; Li, C. C.; Gong, J. L. Controllable Fabrication of Nanostructured Materials for Photoelectrochemical Water Splitting via Atomic Layer Deposition. *Chem. Soc. Rev.* **2014**, *43*, 7469−7484.
(28) Wang, K. X. Z.; Wu, Z. F.; Liu, V.; Brongersma, M. L.; Jaramillo, T. F.; Fan, S. H. Nearly Total Solar Absorption in Ultrathin Nanostructured Iron Oxide for Efficient Photoelectrochemical Water Splitting. *ACS Photonics* **2014**, *1*, 235−240.
(29) Riha, S. C.; Klahr, B. M.; Tyo, E. C.; Seifert, S.; Vajda, S.; Pellin, M. J.; Hamann, T. W.; Martinson, A. B. F. Atomic Layer Deposition of a Submonolayer Catalyst for the Enhanced Photoelectrochemical Performance of Water Oxidation with Hematite. *ACS Nano* **2013**, *7*, 2396−2405.
(30) Resasco, J.; Dasgupta, N. P.; Rosell, J. R.; Guo, J. H.; Yang, P. D. Uniform Doping of Metal Oxide Nanowires Using Solid State Diffusion. *J. Am. Chem. Soc.* **2014**, *136*, 10521−10526.
(31) Sun, K.; Pang, X. L.; Shen, S. H.; Qian, X. Q.; Cheung, J. S.; Wang, D. L. Metal Oxide Composite Enabled Nanotextured Si Photoanode for Efficient Solar Driven Water Oxidation. *Nano Lett.* **2013**, *13*, 2064−2072.
(32) Ling, Y. C.; Wang, G. M.; Reddy, J.; Wang, C. C.; Zhang, J. Z.; Li, Y. The Influence of Oxygen Content on the Thermal Activation of Hematite Nanowires. *Angew. Chem., Int. Ed.* **2012**, *51*, 4074−4079.
(33) Hou, Y.; Zuo, F.; Dagg, A.; Feng, P. A Three-Dimensional Branched Cobalt-Doped α-Fe_2O_3 Nanorod/$MgFe_2O_4$ Heterojunction Array as a Flexible Photoanode for Efficient Photoelectrochemical Water Oxidation. *Angew. Chem., Int. Ed.* **2013**, *52*, 1248−1252.
(34) Katz, M. J.; Riha, S. C.; Jeong, N. C.; Martinson, A. B. F.; Farha, O. K.; Hupp, J. T. Toward Solar Fuels: Water Splitting with Sunlight and "Rust"? *Coord. Chem. Rev.* **2012**, *256*, 2521−2529.
(35) Zandi, O.; Klahr, B. M.; Hamann, T. W. Highly Photoactive Ti-Doped α-Fe_2O_3 Thin Film Electrodes: Resurrection of the Dead Layer. *Energy Environ. Sci.* **2013**, *6*, 634−642.
(36) Klahr, B.; Gimenez, S.; Fabregat-Santiago, F.; Hamann, T.; Bisquert, J. Water Oxidation at Hematite Photoelectrodes: The Role of Surface States. *J. Am. Chem. Soc.* **2012**, *134*, 4294−4302.
(37) Barroso, M.; Mesa, C. A.; Pendlebury, S. R.; Cowan, A. J.; Hisatomi, T.; Sivula, K.; Gratzel, M.; Klug, D. R.; Durrant, J. R. Dynamics of Photogenerated Holes in Surface Modified α-Fe_2O_3 Photoanodes for Solar Water Splitting. *Proc. Natl. Acad. Sci. U. S. A.* **2012**, *109*, 15640−15645.
(38) Mayer, M. T.; Lin, Y. J.; Yuan, G. B.; Wang, D. W. Forming Heterojunctions at the Nanoscale for Improved Photoelectrochemical Water Splitting by Semiconductor Materials: Case Studies on Hematite. *Acc. Chem. Res.* **2013**, *46*, 1558−1566.
(39) Kay, A.; Cesar, I.; Gratzel, M. New Benchmark for Water Photooxidation by Nanostructured α-Fe_2O_3 Films. *J. Am. Chem. Soc.* **2006**, *128*, 15714−15721.

DOI: 10.1021/acsami.5b03298
ACS Appl. Mater. Interfaces 2015, 7, 14072−14078